Effect of overpressure and pulse repetition frequency on cavitation in shock wave lithotripsy

Oleg A. Sapozhnikov and Vera A. Khokhlova
Department of Acoustics, Physics Faculty, M. V. Lomonosov Moscow State University, Moscow 119899, Russia

Michael R. Bailey[a)]
Center for Industrial and Medical Ultrasound, Applied Physics Laboratory, College of Ocean and Fishery Sciences, University of Washington, 1013 Northeast 40th Street, Seattle, Washington 98105

James C. Williams, Jr. and James A. McAteer
Department of Anatomy and Cell Biology, MS 5055, Indiana University School of Medicine, 635 Barnhill Drive, Indianapolis, Indiana 46202-5120

Robin O. Cleveland
Department of Aerospace and Mechanical Engineering, Boston University, 110 Cummington Street, Boston, Massachusetts 02215

Lawrence A. Crum
Center for Industrial and Medical Ultrasound, Applied Physics Laboratory, College of Ocean and Fishery Sciences, University of Washington, 1013 Northeast 40th Street, Seattle, Washington 98105

(Received 8 February 2002; revised 15 June 2002; accepted 20 June 2002)

Cavitation appears to contribute to tissue injury in lithotripsy. Reports have shown that increasing pulse repetition frequency [(PRF) 0.5–100 Hz] increases tissue damage and increasing static pressure (1–3 bar) reduces cell damage without decreasing stone comminution. Our hypothesis is that overpressure or slow PRF causes unstabilized bubbles produced by one shock pulse to dissolve before they nucleate cavitation by subsequent shock pulses. The effects of PRF and overpressure on bubble dynamics and lifetimes were studied experimentally with passive cavitation detection, high-speed photography, and *B*-mode ultrasound and theoretically. Overpressure significantly reduced calculated (100–2 s) and measured (55–0.5 s) bubble lifetimes. At 1.5 bar static pressure, a dense bubble cluster was measured with clinically high PRF (2–3 Hz) and a sparse cluster with clinically low PRF (0.5–1 Hz), indicating bubble lifetimes of 0.5–1 s, consistent with calculations. In contrast to cavitation in water, high-speed photography showed that overpressure did not suppress cavitation of bubbles stabilized on a cracked surface. These results suggest that a judicious use of overpressure and PRF in lithotripsy could reduce cavitation damage of tissue while maintaining cavitation comminution of stones.
[DOI: 10.1121/1.1500754]

PACS numbers: 43.80.Gx [FD]

I. INTRODUCTION

Shock wave lithotripsy (SWL) has proven to be highly successful for the treatment of urinary stones. Indeed, even with the emergence of endourological approaches for stone removal, the majority of calyceal and upper ureteral stones are treated by SWL.[1] Although it is accepted that SWL works very well to break stones, there is increased awareness that shock waves cause collateral damage to the kidney.[2]

Concern over adverse effects has stimulated interest in finding ways to improve lithotripsy. A logical first step toward this goal has been the effort to determine the physical mechanisms of shock-wave action. This work, primarily involving *in vitro* studies, has shown that cavitation plays an important role in stone fragmentation.[3–5] Likewise, cavitation is strongly implicated in causing the hemorrhagic lesion that characterizes SW-induced damage to the kidney.[6–10] Thus, cavitation appears to be involved both in stone comminution and tissue damage.

Several strategies have been proposed to control cavitation in lithotripsy including alteration of the shock pulse to suppress bubble growth and protect tissue,[11] and the use of dual sequential pulses timed to increase the force of bubble collapse and, thereby, enhance stone breakage.[12–16] These strategies are potentially very useful, but they require that physical modifications be made to the lithotripter.

Several studies have explored alternative methods to influence cavitation in SWL. One approach has been to use increased static pressure (overpressure) to minimize cavitation at the focal point of the lithotripter. Delius[17] found that relatively low overpressures had a dramatic protective effect on isolated cells. Maximal cell protection was achieved by overpressure of only ≈1 bar. Overpressure also reduced SW damage to stones, but the effect on cells was much more pronounced. This opens the possibility that if low overpressure could be applied during SWL, tissue-damaging cavita-

a)Electronic mail: bailey@apl.washington.edu

tion in the vasculature might be suppressed without inhibiting stone fragmentation.

Another means to regulate cavitation and one that is available to the urologist at the time of treatment is to change the pulse-repetition frequency (PRF). Increasing the SW delivery rate generates more cavitation bubbles.[18] It has recently been shown that stone fragmentation *in vitro* and *in vivo* is significantly improved by slowing the SW rate.[19] It has also been demonstrated that delivery of SWs at very fast rate increases kidney injury in experimental animals.[20]

These findings suggest that the combined use of overpressure and manipulation of SW rate may result in reduced tissue damage without compromising stone comminution. However, it is difficult to assess the potential value of these strategies or to know how best to apply them because the mechanisms of the overpressure effect and the rate effect are not known. Therefore, we undertook a study involving numerical calculations, ultrasound imaging, and high-speed photography to characterize the effect of low overpressure and SW rate on cavitation bubble dynamics at the focus of an electrohydraulic lithotripter. We tested the hypothesis that increased static pressure and decreased PRF act to reduce cavitation activity by allowing bubbles to dissolve between shock pulses. Bubbles that reside in close contact with the surface of a stone may be stabilized by that interaction and are more resistant to dissolution.[21–23] Thus under conditions of overpressure or low PRF bubbles free within the surrounding medium dissolve between pulses while bubbles that are stabilized within cracks and crevices persist and continue to play a role in stone comminution.

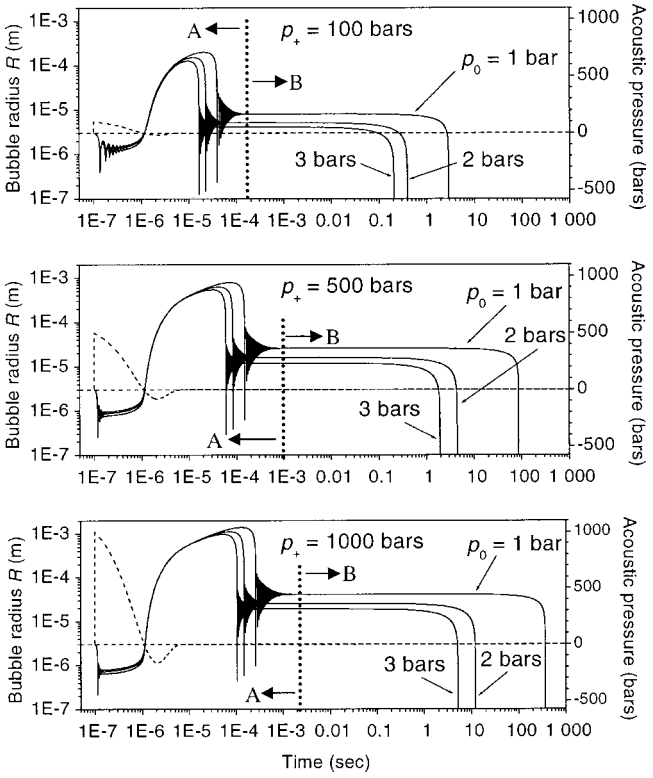

FIG. 1. Calculated $R(t)$ curves (solid lines) for different amplitude shock waves $p_+ = 100$, 500, and 1000 bar and varying static pressure $p_0 = 1$, 2, and 3 bar. Initial bubble radius was $R_0 = 3\ \mu$m. The driving lithotripter wave forms are shown as dashed lines. Time intervals A and B, divided by dotted lines, distinguish different stages in bubble dynamics. The maximum bubble radius and the bubble lifetime increased with p_+ and decreased with p_0.

II. THEORY

A. Basic equations

Our numerical model is the synthesis of a bubble dynamics model created by Church[24] based on the Gilmore equation[25] and a bubble dissolution model described by Epstein and Plesset.[26] As shown in Fig. 1, our model traces the radius of a bubble $R(t)$ over time as the lithotripter pulse sets the bubble into a dramatic growth and collapse followed by a slow dissolution of the bubble. The lifetime of a bubble (t_L^*, the asterisk denotes a calculated value) was defined as the time between the shock wave arrival until the bubble dissolution. The model was used to calculate the lifetime t_L^* as a function of overpressure, initial bubble radius, and shock wave amplitude.

1. Lithotripter pulse model

In the calculations, it was supposed that a small bubble of radius R_0 exists in the medium. A lithotripter pulse arrives at $t=0$ and initiates the bubble dynamics. To represent the wave form radiated by an electrohydraulic lithotripter source, a theoretical temporal profile $p'(t)$ was defined by Church[24] as $p'(t) = p_+ \Theta(t) 2e^{-\alpha t} \cos(\omega t + \pi/3)$, where p_+ is the peak positive pressure of the pulse, $\Theta(t)$ is Heaviside step function, and $\alpha = 9.1 \times 10^5\ \mathrm{s}^{-1}$ and $\omega/2\pi = 8.33 \times 10^4\ \mathrm{s}^{-1}$ are characteristic decay constants. The pulse, modeled after measured wave forms, is a short ($\approx 1\ \mu$s) spike followed by a longer ($\approx 4\ \mu$s) pressure trough, so that the total area of the wave form is equal to zero. The amplitude of the pulse is characterized by the peak positive p_+ pressure which has a fixed ratio with the peak negative p_- pressure $p_+/p_- \approx 6.25$.

2. Bubble dynamics model

In the lithotripsy literature it is common to use a cavitation model based on the behavior of a single spherical bubble.[24] Although this model is somewhat idealistic (in reality a cluster of bubbles exists, and the bubbles are not spherical), it adequately describes many features of the cavitation phenomena.[11,27–29] In this work, the model of a single spherical cavitation bubble (initial radius R_0 between 1 and 30 μm) was employed to study the effect of static pressure ($p_0 = 1-4$ bar) on cavitation in lithotripsy. Note that p_0 is the absolute static pressure and therefore the overpressure in these calculations varied from 0 to 3 bar. Note that pressures are expressed in bar not MPa for convenient comparison to standard atmospheric pressure (1 bar). Fundamental assumptions of the model are as follows: a single bubble exists in an infinite liquid medium; the bubble remains spherical at all times; the interior of the bubble (e.g., temperature, pressure, gas concentration) is spatially uniform; the radius of the bubble is much less than the characteristic length of the acoustic excitation at the corresponding time; body forces (e.g., gravity) have negligible effect on the bubble pulsation; the gas within the bubble behaves as an ideal gas; gas con-

tent in the bubble is changing because of gas diffusion into and out of the surrounding liquid; and vapor pressure in the gas is constant.

The bubble radius $R(t)$ is described by the Gilmore equation,[25]

$$\left(1-\frac{\dot{R}}{C}\right)R\ddot{R}+\frac{3}{2}\left(1-\frac{\dot{R}}{3C}\right)\dot{R}^2 = \left(1+\frac{\dot{R}}{C}\right)H+\left(1-\frac{\dot{R}}{C}\right)\frac{RdH}{Cdt}, \tag{1}$$

where a dot signifies a time derivative, C is the sound speed in the liquid at the bubble wall, and H is the difference between the specific enthalpy in water at the bubble wall relative to the specific enthalpy in the liquid far from the bubble,

$$H=\int_{p_\infty}^{p(R)}\frac{dp}{\rho}. \tag{2}$$

Here $p(R)$ is the pressure in the liquid at the bubble wall and $p_\infty=p_0+p'$ is the pressure, static p_0 plus acoustic p', in liquid far from the bubble. Pressure p and density ρ in the liquid are related by the Tait equation,

$$p=A(\rho/\rho_0)^\Gamma-B, \tag{3}$$

where $A=C_0^2\rho_0/p_0\Gamma$, $B=A-p_0$, Γ is an empirical constant, p_0 is the static pressure in the liquid. The parameters of water were used for further numerical simulations: $\Gamma=7$, the equilibrium density $\rho_0=1000\ \mathrm{kg/m^3}$, the sound speed $C_0=1485$ m/s. From Eqs. (2) and (3), the enthalpy can be expressed in terms of pressure:

$$H=\frac{A^{1/\Gamma}}{\rho_0}\frac{\Gamma}{\Gamma-1}\{[p(R)+B]^{(\Gamma-1)/\Gamma}-[p_\infty+B]^{(\Gamma-1)/\Gamma}\}. \tag{4}$$

The sound speed at the bubble wall, C, can be found from the enthalpy:

$$C^2=C_0^2+(\Gamma-1)H. \tag{5}$$

The pressure in the liquid at the bubble wall is given by

$$p(R)=p_g-\frac{2\sigma}{R}-\frac{4\mu\dot{R}}{R}, \tag{6}$$

where p_g is the pressure of the gas within the bubble, $\sigma=0.0725$ N/m is the surface tension, and $\mu=0.001$ kg/m/s is the coefficient of shear viscosity of water. The gas pressure p_g is proportional to the quantity of gas in the bubble and the gas temperature. Following the method described by Church,[24] we model the complicated bubble dynamics at each temporal step as two elementary separate substeps. At each step, we model the change of bubble radius due to the gas diffusion isothermally and the change of bubble radius due to pressure and inertia adiabatically. The calculation proceeds as follows: first, the bubble radius was modeled as changing isothermally from its current value R to a so-called equilibrium radius R_{0n}, following the change of the gas in the bubble to its current number of moles n; and second, the bubble radius changes adiabatically from the R_{0n} to the new radius R with no change in n.

The first process of bubble radius change due to diffusion takes place slowly under constant static pressure, so that gas pressure is $p_0+2\sigma/R_{0n}$. The equilibrium radius can be found from the equation of the isothermal process in an ideal gas, written for the initial and current parameters of the bubble:

$$\frac{(p_0+2\sigma/R_0)R_0^3}{n_0}=\frac{(p_0+2\sigma/R_{0n})R_{0n}^3}{n}. \tag{7}$$

The solution of this cubic equation can be expressed in the following form:

$$R_{0n}=(a+\sqrt{a^2-b})^{1/3}+(a-\sqrt{a^2-b})^{1/3}-\frac{2\sigma}{3p_0}, \qquad a=\frac{n}{n_0}\frac{R_0^3}{2}\left(1+\frac{2\sigma}{p_0R_0}\right)-\left(\frac{2\sigma}{3p_0}\right)^3, \quad b=\left(\frac{2\sigma}{3p_0}\right)^6. \tag{8}$$

In the second adiabatic process, the equation for R is $p_gR^{3\gamma}=(p_0+2\sigma/R_{0n})R_{0n}^{3\gamma}$, where γ is the adiabatic exponent of the gas. Using Eq. (7), the gas pressure can be written as follows:[24]

$$p_g=\left(p_0+\frac{2\sigma}{R_0}\right)\frac{n}{n_0}\left(\frac{R_0}{R}\right)^{3\gamma}\left(\frac{R_{0n}}{R_0}\right)^{3(\gamma-1)}. \tag{9}$$

The gas diffusion in the liquid is described by the diffusion equation

$$\frac{\partial c}{\partial t}+u\frac{\partial c}{\partial r}=D\frac{1}{r^2}\frac{\partial}{\partial r}\left(r^2\frac{\partial c}{\partial r}\right), \tag{10}$$

where c is gas concentration (the number of moles of gas per unit volume), r is the radial coordinate, u is the radial component of the liquid velocity, and D is the diffusion constant of the gas in the liquid. The constant $D=2.42\times10^{-9}\ \mathrm{m^2/s}$ for air dissolved in water at 20 °C. The liquid can be considered as incompressible most of the time, which gives the following expression for the radial velocity: $u=R^2\dot{R}/r^2$. At the initial time, the concentration of dissolved gas is uniform and equal to c_i. Usually this value is less than the saturated gas concentration c_0 at the initial static pressure p_0. The relative initial concentration can be characterized by the ratio $f=c_i/c_0$. The value of c_0 is related to the static pressure p_0 by Henry's law $c_0=k_Hp_0$, where k_H is a constant. Equation (10) for the dissolved gas concentration $c(r,t)$ has to be solved at $t>0$ and $r>R$. The initial condition is $c(r,0)=c_i$, the boundary conditions are $c(\infty,t)=c_i$ and $c(R,t)=c_s$, where c_s is saturated gas concentration in liquid at the bubble interface. According to Henry's law, $c_s=k_Hp_g$, or, neglecting the dependence of the Henry's constant k_H on temperature,

$$c_s=c_0p_g/p_0. \tag{11}$$

We are interested in calculating the bubble lifetime t_L^*, which includes excitation of the bubble by a lithotripter pulse, consequent expansion, collapse, rebounds, and finally the bubble dissolution due to gas diffusion from the bubble interior to the liquid. The direct numerical solution of Eq. (10) is computationally intensive; therefore appropriate approximations are desired to simplify it. These approxima-

tions have already been used in papers on cavitation and are different for different stages in the bubble cycle.[24,26,30] We use the approximation by Eller and Flynn,[30] as Church[24] did, for region A in Fig. 1 where the bubble radius is rapidly changing, and the approximation by Epstein and Plesset[26] for region B where the static bubble slowly dissolves. The application and appropriateness of the models are discussed in the following with reference to the radius versus time plots in Fig. 1. Church[24] described in more detail the application of the Eller and Flynn model to lithotripsy.

During the time when the bubble is growing and collapsing (region A in Fig. 1), the gas concentration in the liquid varies from the saturated value c_s to the uniform value c_i in a very thin spherical layer near the gas–water interface, because the interface is moving. The thickness of this layer can be estimated from Eq. (10) as $\delta=\sqrt{Dt_*}$, where t_* is a characteristic time. During the first $t_1\approx 3\ \mu$s, the transition layer thickness is on the order of $\delta_1\approx 0.1\ \mu$m, which is much less than the bubble radius at this time, $R_1\approx 3-200\ \mu$m (see Fig. 1). For hundreds of microseconds, the layer continues to grow ($\delta_2\approx 1\ \mu$m), but so does the bubble ($R_2\approx 100-1000\ \mu$m). The use of the inequality $\delta/R\ll 1$ in Eq. (10), as was shown by Eller and Flynn[30] in their first-order approximation, results in the following expression for the number of gas moles in the bubble:

$$n=n_0-4\sqrt{\pi D}\int_0^{\tau}\frac{F(\tau')}{\sqrt{\tau-\tau'}}d\tau', \tag{12}$$

where $\tau=\int_0^t R^4(t')dt'$ and $F=c_s-c_i$.

Bubble growth is followed by collapse and several ''rebounds,'' subsequent growth and collapse cycles. During each of the collapses the radius of the bubble becomes small enough that the assumption $\delta/R\ll 1$ breaks down. However, each collapse stage is short, a small bubble has a small surface area through which diffusion can take place, and so there is little change in the value of n. Therefore we continue to use Eq. (12) throughout the collapse and rebound region to ensure we capture the diffusion at the times when the bubble is large enough—the error induced in the calculation of n will be negligible.[24]

Then, after about $t_m\approx 1$ ms (region B in Fig. 1), the bubble has stopped pulsating. Its equilibrium radius $R_m=R(t_m)$ is larger than the initial bubble radius R_0 because of gas diffusion into the bubble during bubble growth. Now, surface tension, static pressure, and a gas concentration gradient drive gas diffusion from the bubble to the liquid, leading to the bubble dissolution ($n=0$). Eller and Flynn's approximation is not valid during this process. On the other hand, the bubble radius during dissolution varies relatively slowly. Therefore, it is possible to set $u=0$ in Eq. (10). The resulting diffusion equation has an analytical solution in the form of the convolution of the corresponding Green's function with the initial distribution of the dissolved gas concentration. At time $t=t_m$, the diffusion layer thickness δ_m is of the order of several micrometers, so it is still smaller than the corresponding bubble radius ($R_m\geqslant 10\ \mu$m).[24] Therefore, one can use an approximation $\delta_m\to 0$ to simplify the initial condition at $t=t_m: c(r,t_m)=c_i$. The boundary conditions at $t>t_m$ are the same as at $t<t_m: c(\infty,t)=c_i$ and $c(R,t)=c_s$. Then, for the number of gas moles in the bubble,[24] one has

$$\frac{dn}{dt}=-4\pi R^2 D(c_s-c_i)\left(\frac{1}{R}+\frac{1}{\sqrt{\pi D(t-t_m)}}\right). \tag{13}$$

Note that at small time $t-t_m$, Eq. (13) gives the same expression for dn/dt as Eq. (12) at small t. However for larger time, these equations differ substantially. In Eq. (13) it is not assumed that the diffusion layer is thin.

During the slow changes of the bubble size, the gas temperature can be considered as a constant value equal to the liquid temperature T_0. The isothermal gas process is governed by

$$p_g\tfrac{4}{3}\pi R^3=nGT_0, \tag{14}$$

where $G=8.31$ m^3 Pa/mol K is a universal gas constant. The bubble radius no longer needs to be modeled by the dynamic equations [Eqs. (1)–(9)], instead one can use the quasistatic equation:

$$p_g=p_0+\frac{2\sigma}{R}. \tag{15}$$

Equations (13)–(15) give the following equation for the bubble radius:

$$\frac{dR}{dt}=-K\frac{1-f+\dfrac{2\sigma}{p_0R}}{1+\dfrac{4\sigma}{3p_0R}}\left(\frac{1}{R}+\frac{1}{\sqrt{\pi D(t-t_m)}}\right), \tag{16}$$

where $K=GT_0Dk_H^{-1}$ and $f=c_i/c_0$. The initial condition is $R=R_m$ at $t=t_m$. Note that the choice of the value of t_m is somewhat arbitrary: t_m should be larger than the time when the bubble rebounding finishes, but much smaller than the lifetime t_L. In the case of bubble behavior in the lithotripter field, the choice $t_m=1$ ms is reasonable. The right-hand side of Eq. (16) has singularities at $t\to t_m$ and when $R\to 0$. These singularities can be avoided by calculating the value of $\xi=\sqrt{t-t_m}$ as a function of R, instead of considering R as a function of t. The equation for $\xi=\xi(R)$ follows from Eq. (16):

$$\frac{d\xi}{dR}=-\frac{\sqrt{\pi D}}{2K}\frac{R\left(R+\dfrac{4\sigma}{3p_0}\right)}{(R+\xi\sqrt{\pi D})\left[R(1-f)+\dfrac{2\sigma}{p_0}\right]}. \tag{17}$$

The function $\xi(R)$ is to be calculated when the bubble radius changes from $R=R_m$ to $R=0$ to complete dissolution of the bubble. The initial condition is $\xi(R=R_m)=0$.

Therefore, Eq. (1) was solved numerically to calculate rapid bubble motion, and Eq. (17) was then solved to calculate the slow bubble dissolution. To solve for fast bubble motion, Eq. (1) was written as two first-order differential equations for bubble wall radius R and velocity dR/dt. A fifth-order Runge–Kutta algorithm with adaptive step-size control was used on a nonuniform time grid $\Delta t(t)$ that followed the dynamics of the bubble.[31] Equation (12) was integrated simultaneously on the same time grid and yielded a

calculation of gas diffusion during rapid motion. The number of moles n, the derivative dn/dt, equilibrium bubble radius R_{0n}, and gas pressure in the bubble p_g were calculated at each time point t for use in solving Eq. (1) at the next time step. The values of p_g and R_{0n} were obtained explicitly using Eqs. (8) and (9) from the known values of R and n. The derivative dn/dt was calculated using backward finite difference with the solutions for n at the current and previous time points. However, the solution for the number of moles n, Eq. (12), is implicit, as it depends on not-yet-known values of p_g and R_{0n}. An iterative procedure was employed at each time point to calculate $n \rightarrow R_{0n} \rightarrow p_g \rightarrow n \rightarrow \cdots$.[24] Initial values of R_{0n} and p_g for iteration were obtained from the number of moles, $n + dn/dt\,\Delta t$, extrapolated linearly from the previous time point. Linear extrapolation for n was also used for the Runge–Kutta evaluations within the full time step. Run times for each $R(t)$ curve were less than 10 min on a Compaq XP1000 workstation. During the second slow stage of bubble dissolution, Eq. (17) was solved numerically by fourth-order Runge–Kutta algorithm. Parameter values chosen were for water at laboratory conditions: $\sigma = 0.0725$ N/m, $\mu = 0.001$ N s/m^2, $\rho_0 = 1000$ kg/m^3, $C_0 = 1485$ m/s, $T_0 = 20\,^\circ$C, $\gamma = 1.4$, and $k_H = 0.782 \times 10^{-5}$ mol/m/N.

The value of initial gas concentration in water is an important parameter in studying the effect of overpressure. Two limiting cases can be considered. In one limiting case, the water has been given sufficient time (and mixing) at overpressure to become saturated: absolute gas concentration c_i increases proportionally with p_0, such that the relative gas concentration $f = 1$ for all p_0. In the other limiting case, the ambient pressure changes quickly so that c_i is constant, and f varies inversely proportionally with p_0. Our experiments closely modeled the latter case because our system had very small gas/water interfaces through which air could diffuse. Therefore, all simulations were performed assuming a fast change of the pressure p_0. Initial gas concentration c_i in water was taken equal to the saturation value at atmospheric conditions, $c_i = c_0(p_0 = 1\text{ bar}) = 0.7899$ mol/m^3, which corresponds to $f = 1$ for $p_0 = 1$ bar and $f \propto 1/p_0$. The effect of variable f has been explored by Epstein and Plesset,[26] and as might be expected, the lower the concentration of air in the water the faster the bubble dissolves.

B. Theoretical results

Calculated $R(t)$ curves describing the bubble life are shown in Fig. 1 for a bubble with initial radius 3 μm. Calculations are shown for shock waves with peak acoustic pressures $p_+ = 100$, 500, and 1000 bar and for absolute static pressure $p_0 = 1$, 2, and 3 bar. The bubble radius curves are solid, and each dashed line represents the acoustic pressure of the lithotripter pulse driving the bubble. All axes except acoustic pressure are plotted in logarithmic scale. It is seen that the initial positive-pressure spike of the lithotripter pulse results in a rapid constriction of the bubble to a radius of less than 1 μm (the first collapse). Then, the negative-pressure phase of the lithotripter pulse initiates the growth of the bubble. The inertia imparted to the liquid surrounding the bubble is sufficiently large that the bubble continues to grow after the lithotripter pulse has passed. Growth continues for a relatively long period (in excess of 100 μs). Eventually, the static pressure in the fluid forces the bubble to collapse again. We denote the time of this inertial collapse as t_c^*. At about 1 ms, after a series of rebounds (subsequent smaller growth and collapse cycles), the bubble attains a stable radius referred to by Church as the ''time-varying equilibrium radius.''[24] The term equilibrium radius is used here, too, although the radius is changing slowly as the bubble dissolves. The equilibrium radius is larger than the initial radius, because during the expansion phase of the bubble, the gas concentration within the bubble is low, and gas from the surrounding liquid diffuses into the expanded bubble. However, the nonpulsating bubble slowly dissolves, the bubble radius tends to zero, and finally, the bubble disappears. This time t_L^* defines the bubble lifetime.

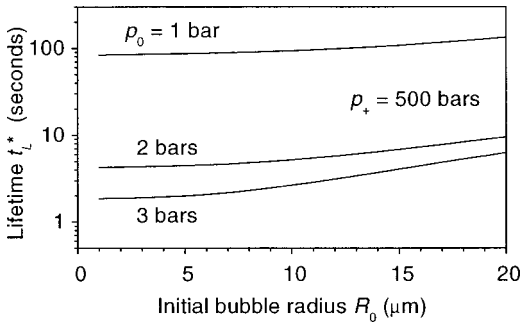

FIG. 2. Calculated bubble lifetime t_L^* for $p_+ = 500$ bar as a function of initial bubble radius R_0 for $p_0 = 1$, 2, and 3 bar. Lifetime, which starts with arrival of the lithotripter pulse and ends with bubble dissolution, is fairly insensitive to R_0 especially in the range 1–10 μm.

For a given shock amplitude one can observe that the static pressure has a negligible effect on bubble dynamics during the first 10 μs. The strong negative acoustic pressure of the lithotripter pulse drives the bubble at this period. The peak positive ($p_+ = 100$–1000 bar) and negative ($p_- = 16$–160 bar) pressure amplitudes in the lithotripter pulse are much greater than p_0 (1–3 bar).

After the lithotripter pulse has passed, the static pressure becomes the main factor driving the inertial behavior of the bubble. As a result, the increase in p_0 gives rise to a shortening of the collapse time t_C^*, a decrease in maximum bubble radius, and an increase in minimum radius. The equilibrium radius decreases and the lifetime t_L^* shortens for higher p_0.

The lifetime t_L^* shows how fast cavitation bubbles dissolve—these bubbles are potential nucleation seeds for cavitation during a subsequent shock wave. The lithotripter pulse repetition period ($T = 1/\text{PRF}$) is of the order of $T = 1$ s. If the lifetime exceeds this value, the cavitation bubbles do not have enough time to dissolve between successive pulses, and the cavitation should be very pronounced. If, however, $t_L^* < T$, then the cavitation seeds dissolve before the next shock wave arrives, and one would expect that cavitation may be diminished. It is instructive, therefore, to study how the lifetime t_L^* depends on various parameters, in particular, on initial bubble radius, R_0, static pressure, p_0, and the lithotripter pulse peak pressure, p_+.

Figure 2 shows curves for lifetime *versus* initial bubble

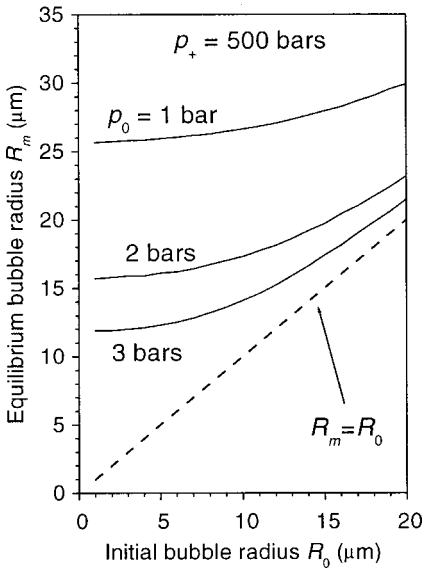

FIG. 3. Equilibrium bubble radius R_m at 1 ms following growth and collapse, as a function of initial bubble radius R_0 for $p_+=500$ bar and $p_0=1$, 2, and 3 bar. Radius R_m is fairly insensitive to R_0 especially in the range 1–10 μm.

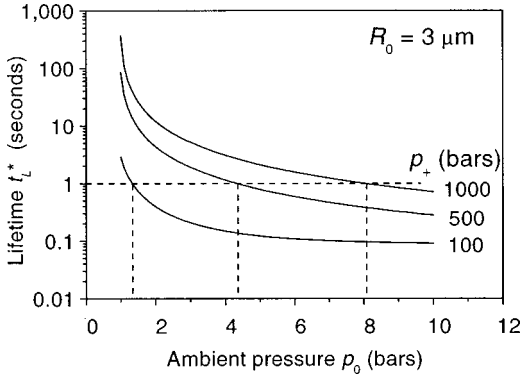

FIG. 4. Calculated lifetime t_L^* vs static pressure p_0 for initial bubble radius $R_0=3$ μm and $p_+=100$, 500, and 1000 bar. Larger negative pressure excursions p_-, corresponding to increased p_+, cause longer and larger bubble growth, which creates increased gas influx, larger R_m, and longer lifetime. The lifetime decreased dramatically with increased static pressure p_0 and with decreased lithotripter pulse amplitude p_+. The horizontal dashed line marks the pulse repetition period of 1 s, which corresponds to a typical clinical rate of 1 Hz. The vertical dashed lines indicate the corresponding static pressure for the different positive peak pressures.

radius at different static pressures p_0. The lithotripter pulse peak pressure equals $p_+=500$ bar. One can see from these curves that lifetime is fairly insensitive to the initial bubble size, especially if $R_0<10$ μm. This insensitivity is in agreement with the results of Church,[24] who calculated that the $R(t)$ curves for a bubble in a lithotripter are practically identical for different R_0. As a result, the amount of the gas that diffuses into the bubble during the relatively long period of its inertial behavior is also insensitive to the value of R_0. Note that the amount of diffused gas exceeds the initial amount of gas in the bubble by a factor of $10–10^4$. Therefore, gas diffusion makes the equilibrium bubble radius after the inertial collapse and rebounds, R_m, fairly independent of R_0. The corresponding curves for R_m vs R_0 calculated at $t=1$ ms are shown in Fig. 3. For small values of R_0, the slopes of the curves are nearly zero; in other words, many values of R_0 produce roughly the same R_m. For larger values of R_0 the amount of diffused gas becomes smaller than the initial amount of gas in the bubble, and R_m asymptotically approaches R_0. For higher static pressures the influence of the initial bubble radius starts at smaller values of R_0.

Figure 4 shows the lifetime t_L^* *versus* static pressure p_0 for different lithotripter pulse amplitudes p_+. Since t_L^* depends only weakly on initial bubble radius, R_0 in all calculations was 3 μm. At $p_0=1$ bar, t_L^* ranges from 3 to 400 s. Larger p_-, corresponding to increased p_+, caused the bubble to grow larger and last longer before it collapsed. The larger, longer growth causes more gas infusion into the bubble, which creates a larger bubble R_m after growth and collapse. The larger bubble subsequently takes longer to dissolve. It is seen that lifetimes quickly decrease with increase of static pressure. At $p_0=4$ bar, the range of t_L^* values is reduced to 0.2–3 s, more than one order of magnitude less than for $p_0=1$ bar. Absolute values of t_L^* are subject to initial gas saturation levels f and the accuracy of the lithotripter pulse model; however modest overpressures two orders of magnitude less than p_+ or p_- strongly reduce t_L^*. Figure 5 shows that for peak pressures p_+ (ordinate) less than 320 bar and static pressure $p_0=3$ bar, t_L^* is less than 1 s. Therefore for a standard clinical exposure (320 bar, 1 Hz),[32] increasing the static pressure to 3 bar means bubbles created by one pulse dissolve before the next pulse arrives.

III. EXPERIMENTS

A. Materials and methods

1. Lithotripters

A Dornier HM-3 electrohydraulic lithotripter (Dornier Medical Systems, GmbH) was used for the pipette experiments shown in Fig. 10. All other experiments were conducted in a research lithotripter patterned after the Dornier HM-3 lithotripter.[32] Refurbished Dornier electrodes (Service

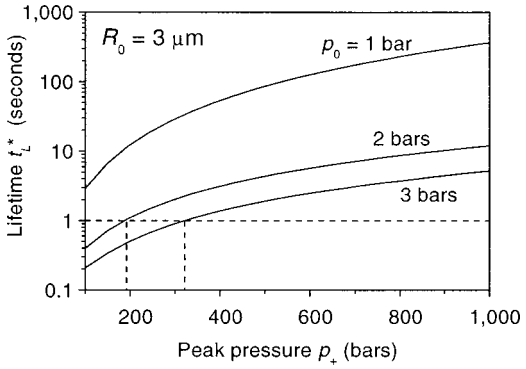

FIG. 5. Calculated lifetime t_L^* vs lithotripter pulse amplitude p_+ for $p_0=1$, 2, and 3 bar, $R_0=3$ μm. Lifetimes are higher for stronger acoustic driving pressures, because the bubble grows larger. Static pressure accelerates dissolution primarily by increasing the gas concentration gradient across the gas–liquid interface. At the clinical lithotripsy conditions $p_+=320$ bar and PRF=1 Hz, static pressure $p_0=3$ bar (bubble lifetime $t_L^*<1$ s) causes bubbles to dissolve between pulses. The horizontal dashed line marks the pulse repetition period of 1 s, which corresponds to a typical clinical rate of 1 Hz. The vertical dashed lines indicate the corresponding positive peak pressures for the different static pressures.

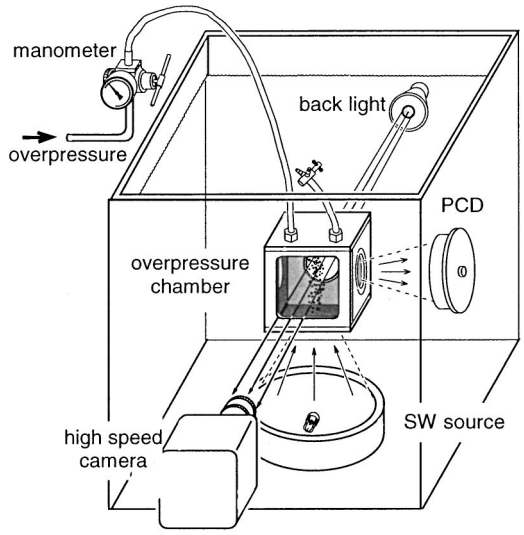

FIG. 6. Experimental setup with the pressure cube. A high-speed camera recorded backlit images of the bubbles through a glass window. A thin mylar window in the cube enabled detection of acoustic emissions from collapsing bubbles with a passive cavitation detector (PCD)—Ref. 33. Lithotripter pulses passed through a polyphenylene oxide (PPO) plate that was acoustically well-matched to water (Ref. 32).

Trends, Kennesaw, GA) were used. Dimensions of the brass ellipsoidal reflector were half major axis $a=13.8$ cm and half minor axis $b=7.75$ cm. The reflector was 1.3 cm short of being a semiellipsoid. Charging potentials 18, 20, and 24 kV were used, and the capacitance was 80 nF. Water was de-ionized and NaCl was added to reach a conductivity of 600 μS/cm. Water was degassed to 4 ppm of oxygen. Water temperature was 37 °C in the clinical bath and 22 °C in the research bath. Peak positive pressures at 18 kV charging potential were 350 ± 80 bar (mean$\pm$standard error for $N=10$ measurements) measured with a Reference Shock Wave Hydrophone (Sonic Industries, Hatboro, PA). Higher charging potential produced larger positive and negative pressures. Cleveland *et al.*[32] described in more detail the design and acoustic output of the research lithotripter.

Lithotripter pulses were triggered at several pulse repetition frequencies (PRFs). The slowest PRF, referred to as the slow rate, was single pulses triggered minutes apart. Clinically relevant rates of 0.5, 1, 2, and 3 Hz were also investigated. Measurements were made on the last of ten pulses triggered at these rates.

2. Containers and pressure chambers

Measurements were made of cavitation in water in pressure chambers placed in the lithotripter. Three types of containers were used: a polyethylene terephthalate (PETE) soda bottle (''pressure bottle'')[33] with a flange, 4 mL, low-density polyethylene pipette bulbs (Sigma Chemical Company, St. Louis, MO), and a plastic chamber (''pressure cube'') with glass and mylar ports (2.5 cm diameter) for optical and acoustic windows.[23] The length, diameter, and wall thickness of the approximately cylindrical pressure bottle were 130, 80, and 0.3 mm and of the pipette bulb were 42, 15, and 0.5 mm. The experimental setup with the pressure cube is shown in Fig. 6. A 12.7-mm-thick polyphenylene oxide (PPO) bottom plate on the chamber transmitted the lithotripter pulses with negligible change of wave form or amplitude at the focus.[34] The top plate was made of the same material, and negligible reflection was measured. Compressed air (1–3 bar gauge) was used to pressurize each chamber. Pressure was elevated for 1 min before measurements were made. The water–air interface was small to minimize gas diffusion into the water and was contained in the 0.25 in. (6.4 mm) inner diameter of the pressure tubing. Hose barbs, quick disconnect pressure fittings, and plastic wire ties were used to connect segments of tubing and pipettes. The water in the chambers was taken from the lithotripter water bath.

3. High-speed photography

Cavitation in the water tank was filmed with a Kodak Ektapro 4540 high-speed digital camera (Eastman Kodak Company, Rochester, NY) at a rate of 40 500 frames/s (i.e., each frame was exposed for 25 μs). We used a 24–120 mm lens with and without a 2×-magnifying lens. The focal area was backlit with a 1000 W lamp and was filmed through the acrylic wall of the tank. The sensor had 64×64 pixels, and images were presented in 256 grayscale levels. The 10 or 20 mm square images (30 mm depth of focus) captured the cluster of bubbles growing and collapsing along the lithotripter axis which ran from lower right to upper left in the image. Images were stored on VHS videotape. Video images were digitized from videotape and analyzed with NIH Image (Bethesda, MD) on a Macintosh G3 computer. The images in Fig. 12 were acquired with an Imacon 200 high speed camera (DRS Hadland, Cupertino, CA) and stored digitally. A 1000 J flash lamp provided lighting from the front, and exposure times were 100 ns/frame. Interframe spacing was 50 μs, and the camera resolution was 1280 by 1024 pixels. In Fig. 12, two images are shown selected from many 15-image movie sequences.

4. Passive cavitation detection

A passive acoustic cavitation detector (PCD) recorded the shock waves emitted during bubble collapse.[35,36] The concave piezoceramic sensing element had a radius of curvature of 200 mm, an aperture diameter of 100 mm, and a resonance frequency of 1.08 MHz. The acoustic axes of the lithotripter and the PCD were perpendicular and confocal. The output signal was high-pass filtered (300 kHz) to remove noise created by excitation of a radial resonance of the sensing element. Signals were demodulated to remove 1 MHz ringing by the PCD. The PCD has been calibrated[35] for cavitation bubble collapses, and a filtered PCD signal of 1 V corresponds to an acoustic emission from a bubble with amplitude 9.5 MPa at 10 mm from the center of the cavitation bubble.

The PCD signal typically consisted of two spikes. The first spike occurred when the lithotripter pulse first interacted with any bubbles initially present in the focal region. The spike resulted from nonlinear scattering from bubbles (i.e., a combination of simple scattering and sound generated by the bubble motion). The bubbles then grew and collapsed. A sec-

ond spike was emitted when the collapse halted. The time between the spikes associated with the growth and collapse is referred to as the collapse time t_C.

Both the PCD and the high-speed camera were simultaneously triggered by a photodetector[32] that detected the spark discharge that initiated the lithotripter pulse. The discharge occurred at time $t=0$. The lithotripter pulse arrived at the focal point $F2$ after 180 μs because it traveled the length of the major axis $2a=276$ mm at a sound speed $C \approx 1.5$ mm/μs. The high-speed camera first recorded bubbles in the frame (each frame was 25 μs in duration) at $t=180$ μs. The PCD had an extra delay of the acoustic travel time from $F2$ to the PCD element (200 mm/1.5 mm/μs $=133$ μs). In PCD measurements presented in this paper, the 133 μs delay has been subtracted from the time axis for easier comparison to camera images.

5. Diagnostic ultrasound

B-mode ultrasound images were obtained using a clinical Bruel and Kjaer 3535 diagnostic ultrasound scanner and a 7.5 MHz curved scan head (model 8545). The frame rate was 34 frames/s, and the displayed mechanical index [MI = derated peak negative pressure (MPa) over the square root of the frequency (MHz)] was 0.8. The scan head was mounted rigidly in the water such that the lithotripter axis was at the 5 cm depth of the image where the scanner was focused. Images were recorded to videotape and later transferred to a Macintosh G3 for analysis. NIH Image software was used to quantify the length of time that echogenic regions on the image persisted. Histograms of pixel-grayscale level were measured for a sequence of image frames. Times were determined by the number of consecutive frames containing pixels within the region of interest brighter than a threshold value.

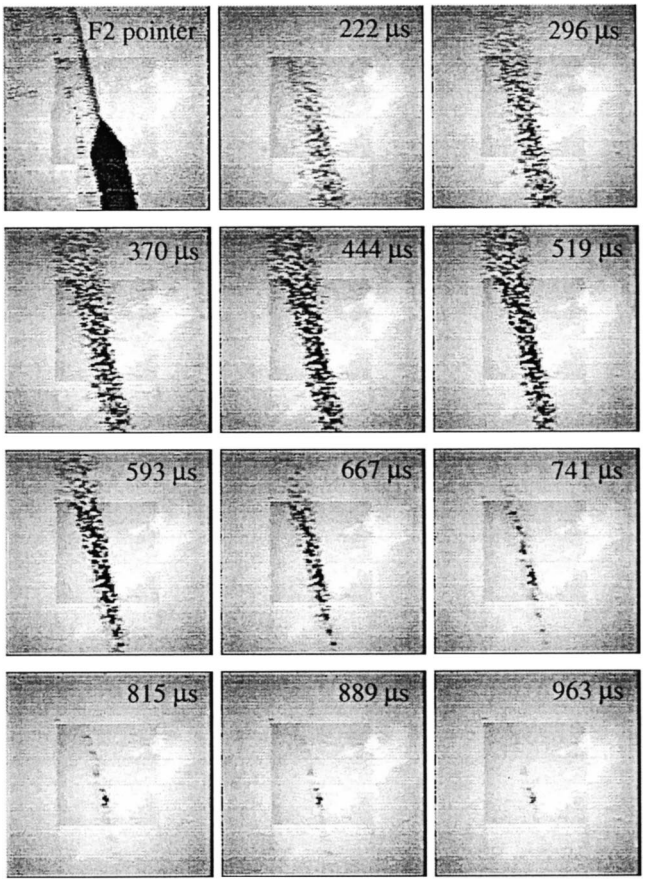

FIG. 7. A time sequence of high-speed photographs of cavitation produced by the lithotripter. The pointer in the first frame (upper left) marks the focal point of the lithotripter and shows the direction of acoustic propagation along the lithotripter axis. Each frame shows a 7.25 by 7.25 cm field of view. A cylindrical cluster ($\approx 1.5\times > 8$ cm) of bubbles formed and collapsed to a 1.5 mm thin line in about 500 μs. Lithotripter charging potential was 24 kV, $p_0=1$ bar, and PRF=1 Hz.

B. Experimental results

1. Free field

The lithotripter created a cylindrical cluster of cavitation bubbles.[11,36,37] Figure 7 shows the cluster in a sequence of high-speed frames. In the first frame, a pointer indicates the geometric focus $F2$ of the lithotripter and the direction of pulse propagation along the lithotripter axis. The remaining frames show the result of the last lithotripter pulse in a sequence of ten lithotripter pulses triggered at 1 Hz and 24 kV. Static pressure p_0 was 1 bar. At 222 μs (42 μs after the shock wave arrived at the focus) a cluster of bubbles was starting to grow along the shock wave axis. The bubbles grew in size, and the cluster reached dimensions of 1.5 cm in diameter by greater than 8 cm in length (frames at 444 and 519 μs). The cluster then collapsed to a narrow line of bubbles (frame at 741 μs) after more than 500 μs. The last two frames showed ''rebound'' or secondary growth and collapse of the cluster.[35]

2. Overpressure

Overpressure dramatically suppressed bubbles as seen in Fig. 8. Both images show the pressure bottle[33] positioned in the lithotripter field. In the top frame, pressure in the bottle and in the surrounding water was 1 bar, and the field was very similar to that in Fig. 7 without the bottle. In the bottom frame, static pressure in the bottle had been increased to 4 bar, and no bubbles were seen in the bottle.

Acoustic emissions from the bubbles were observed to correlate with collapses of the bubble cluster. Figure 9 shows video images of the cluster and simultaneous PCD measurements recorded in the pressure cube. At $p_0=1$ bar, a large dense cluster grows and collapses in $t_C \approx 350$ μs. A strong spike was recorded by the PCD at 180 μs when bubbles were first seen in the images and again ≈ 350 μs later when the bubbles collapsed. Timing agreement was excellent. At $p_0=1.5$ bar, very sparse and short-lived bubbles appeared. Very little signal was detected by the PCD, likely because few bubbles existed at the PCD focus. When a two-spike signal was detected, t_C was less than 200 μs. This reduction in t_C with overpressure was in good agreement with calculations and measurements reported by Cleveland *et al.*[22] and our calculations in Fig. 1. An increase in static pressure of only 0.5 bar significantly reduced the number of bubbles seen, the measured collapse times t_C of the bubbles, and the signal detected by PCD.

An ultrasound scanner and a pressurized pipette bulb were used to investigate the reduction in bubble density by

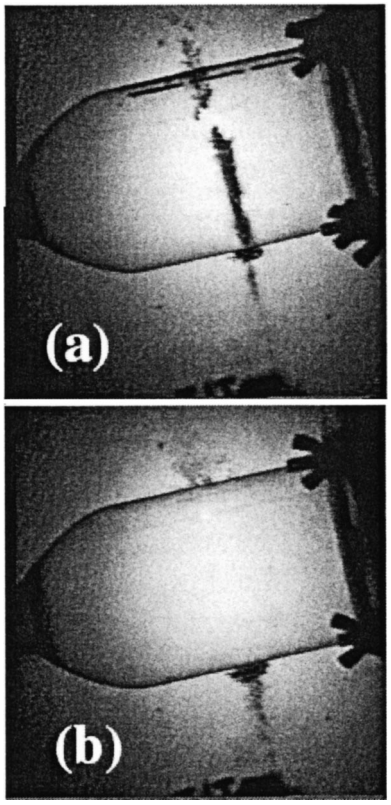

FIG. 8. High-speed images in and around a polyethylene terephthalate (PETE) bottle. Pressure in the bottle was $p_0=1$ bar (a) and 4 bar (b); outside the bottle $p_0=1$ bar in both cases. In the pressurized bottle, no bubbles were seen. Good acoustical transmission is evidenced by the presence of a cavitation cluster on both sides of the bottle. Lithotripter charging potential was 18 kV and PRF=1 Hz.

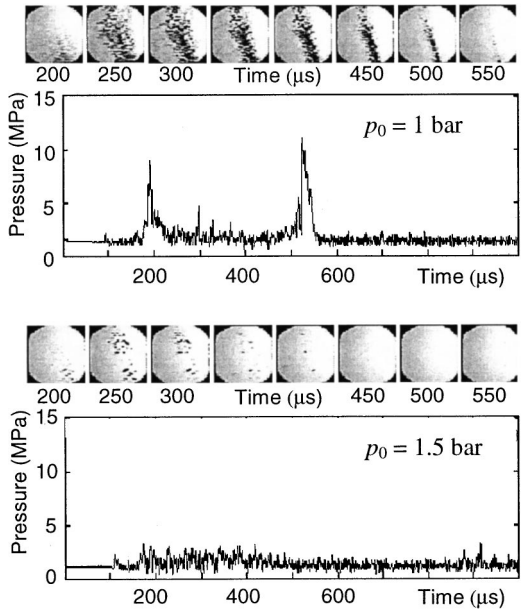

FIG. 9. Simultaneous high-speed camera images and passive cavitation detection for $p_0=1$ bar and 1.5 bar, charging potential 18 kV, and PRF $=1$ Hz. At $p_0=1$ bar, a dense cluster of bubbles grew and bubbles collapsed. The PCD spikes bracketed the growth and collapse; $t_C\approx 350$ μs. At $p_0=1.5$ bar, few bubbles were seen and little signal was detected. Bubbles and signal lasted less than 200 μs. The overpressure of only 0.5 bar dramatically reduced the number and the lifetime of the cavitation bubbles.

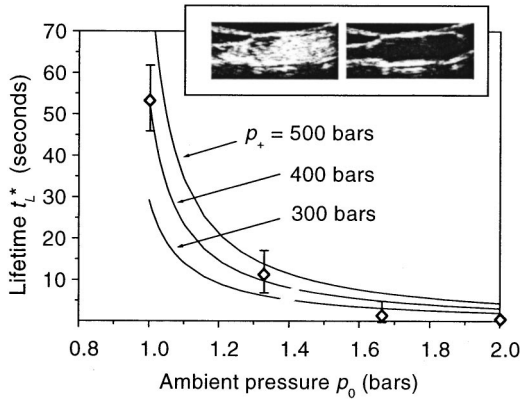

FIG. 10. Comparison of calculations and measurements of the bubble lifetime vs p_0. Measured lifetime t_L (diamonds) was determined from the presence of hyperechogenicity in *B*-mode-images of the pipette. Calculated lifetime t_L^* (solid line) is shown for shock wave amplitudes that cover the variation in the shock waves generated by this lithotripter.

overpressure. The scanner imaged from the top of the bulb and the lithotripter pulse propagated from the right in the inset images in Fig. 10.[22] Pipette bulbs were filled with nondegassed water, and single lithotripter pulses (18 kV) were fired. The ultrasound scanner was too slow to detect the t_C, but it displayed bright echoes likely from residual bubbles,[22,38,39] which were too small to be seen in the high-speed camera images after bubble collapse. The inset in Fig. 10 shows ultrasound images at $p_0=1$ bar (left) and $p_0=2$ bar (right), 1 s after pulse arrival. The echogenic cloud that filled the pipette at atmospheric pressure ($p_0=1$ bar) was subsequently seen to dissipate by $t=60$ s. At $p_0=2$ bar, no bright echoes were detected in ultrasound images of the pipette. This result indicates that overpressure either suppressed bubble growth altogether, or the lifetime of the bubbles was too short to be recorded.

Figure 10 shows a plot of bubble lifetime versus p_0. Figure 10 compares the calculated lifetime t_L^* for selected shock wave amplitudes (solid lines) with the measured lifetime t_L of hyperecho in the pipette (diamonds). An initial radius of $R_0=3$ μm was used in the calculations, but recall that the calculations were not very sensitive to initial bubble size. Peak pressures of the pulses were $p_+=384\pm 62$ bar and $p_-=100\pm 14$ bar (mean$\pm$standard error for $N=10$ measurements)[32] but could not be recorded simultaneously with the measurement. Curves were calculated for three values of p_+ to cover the range of p_+ produced by interspark variation. Lifetime t_L measured on *B*-mode ultrasound image was the time between the interference caused by spark discharge and hyperecho dissipation and was quantified on digitized video frames as described in Sec. III A. Both measured t_L and calculated t_L^* decay quickly with increasing static pressure and are in excellent qualitative agreement with each other. The dissolution time in the experiment was slightly less than in the calculations for large overpressure.

3. Pulse repetition frequency

High-speed camera images were collected for $p_0=1$, 1.5, and 2 bar, and PRF=0.5, 1, 2, and 3 Hz. Figure 11 shows the images recorded at one half of the time for the

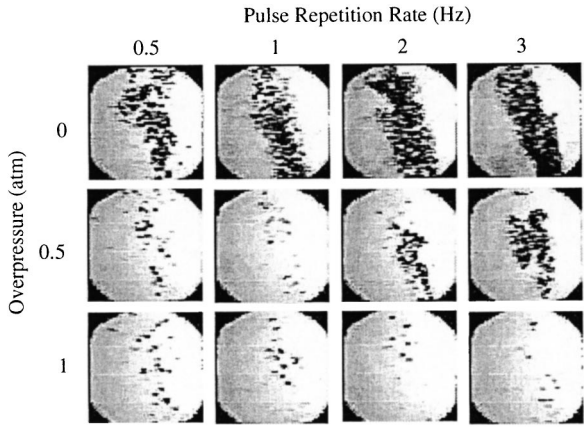

FIG. 11. High speed images of the peak bubble cloud as a function of overpressure and pulse repetition frequency (PRF). At $p_0=1$ bar (top), bubbles did not dissolve between pulses and a dense bubble cluster is apparent for all the PRFs getting more dense with increasing PRF. At $p_0=2$ bar (bottom), bubbles did dissolve between pulses and a sparse bubble cluster is apparent for all the clinical PRFs. At $p_0=1.5$ bar (center), 2 and 3 Hz were fast enough rates to create a dense cluster, but 0.5 and 1 Hz were too slow. Hence, the lifetime t_L at $p_0=1.5$ bar was greater than $(1\text{ Hz})^{-1}=1$ s but less than $(2\text{ Hz})^{-1}=0.5$ s. These images show that increased static pressure and PRF can be used together to suppress cavitation.

second collapse $t_C/2$. Charging potential was 18 kV. At zero overpressure ($p_0=1$ bar), all four rates produced a dense cluster of bubbles in water. By visual inspection, cluster density appeared to increase with increased PRF. At 0.5 bar overpressure ($p_0=1.5$ bar), bubbles were sparse at PRF $=0.5$ and 1 Hz, but dense at 2 and 3 Hz. At overpressures of 1 bar and above, the field was sparse for all the tested PRFs. This result indicates that bubble lifetime was greater than 2 s at atmospheric pressure, was in the range of 0.5–1.0 s at 1.5 bar, and was less than 0.33 s at 2 bar. These values agree well with the measured values in Fig. 10 and are slightly lower than the calculated values. The similarity indicates that the ultrasound is able to detect bubbles that cause cavitation seen with the camera, and that p_0 and PRF can be used together to suppress cavitation.

The denser clouds at higher PRF had smaller bubbles and longer t_C. In Fig. 12, a cavitation cluster created at 2 Hz (top) is compared to that created at 3 Hz (bottom). Maximum on-axis bubble diameter was 1.8 ± 0.2 mm at 1 Hz, 1.5 ± 0.3 mm at 2 Hz, and 0.8 ± 0.2 mm at 3 Hz. The largest bubble was selected from six image sequences at each frequency. The t_C was 225 ± 35 μs at 1 Hz, 336 ± 45 μs at 2 Hz, and 430 ± 40 μs at 3 Hz (six samples each). Measurement of t_C was by PCD signal recorded simultaneously with camera imaging. Collapse times determined from camera images agreed to within the interframe resolution of 50 μs.

4. Stabilized bubbles

The appearance of a few bubbles following a single lithotripter pulse or at $p_0=2$ bar and possible differences between liquids warrant investigation of stabilizing effects. Apfel,[21] Atchley and Prosperetti,[40] and Crum[41] among others have developed a ''crack and crevice model'' for how bubbles trapped within solid particles are stabilized against overpressure, surface tension, and dissolution. Bubble stabilization particularly that by cracks in a solid is pertinent to why overpressure suppresses damage to suspended cells but has little effect on kidney stone comminution.[17,22,23,42]

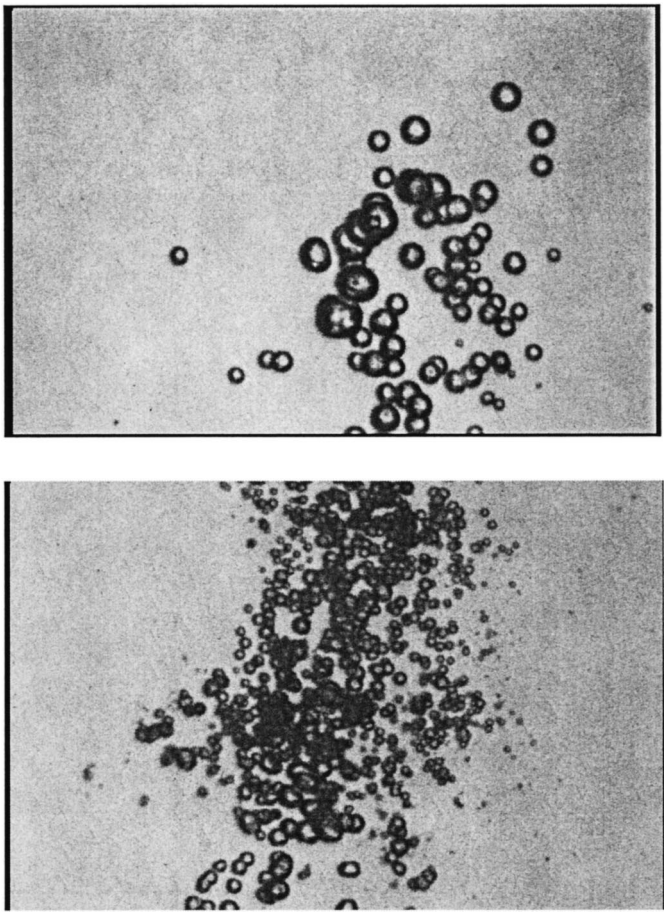

FIG. 12. Cavitation cluster created at 2 Hz (top) and 3 Hz (bottom). The width of the image is 29 mm. The denser cloud, created at higher PRF, contained smaller bubbles. The time to bubble collapse was also longer.

Stabilization of bubbles by cracks was investigated with a glass microscope slide before and after it cracked. The PETE bottle pressure chamber[33] was used, and the slide fit across the diameter of the bottle as shown in Fig. 13. The transparency of the glass enabled back lighting and visualization of the cluster of bubbles on both sides of the slide. Figure 13 shows camera images of the cluster produced at $p_0=1$ bar (top) and at $p_0=4$ bar (bottom) before (left) and after (right) a crack formed in the glass slide. Charging potential was 18 kV, and PRF was 1 Hz. At $p_0=1$ bar, a dense cluster of bubbles was seen in both cases. The cluster was slightly bulbous at the interface with the glass. The crack can be seen in the center of the bulge. At $p_0=4$ bar, no bubbles were seen on the crack-free glass (left) or in the free-field surrounding the cracked glass. But at the crack, bubbles can be seen. These data indicate that overpressure suppressed cavitation in the free field but not at the crack in this solid object. It is important to note that the crack shown in this image was caused by shock wave treatment while the slide was immersed in the water within the lithotripter tub. Thus, the crack could not have been filled *a priori* with gas. It appears, therefore, that the crack may have served to attract, then stabilize cavitation nuclei.

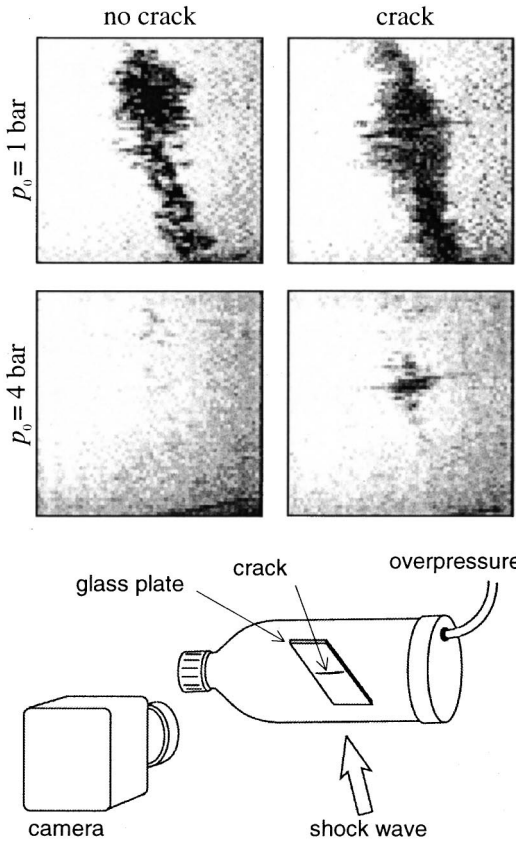

FIG. 13. Images (3.8 cm per side) of the bubble cluster produced at $p_0 = 1$ bar (top) and at $p_0 = 4$ bar (bottom) before (left) and after (right) a crack formed in the glass slide. At 4 bar the cavitation was suppressed in the free-field but was persistent at the crack. Charging potential was 18 kV, and PRF was 1 Hz.

IV. CONCLUSIONS

It is now well established that a typical clinical exposure of 2000 lithotripter pulses causes collateral damage, primarily vascular trauma, to the kidney.[2] The precise physical acoustic mechanisms responsible for this injury have yet to be determined, but there is good evidence to suggest that cavitation is involved. During SWL, cavitation has been detected *in vivo* by ultrasonography[38] and single transducer PCD.[7] In recent studies simultaneous dual-PCD and *B*-mode ultrasound followed by dual-source high intensity focused ultrasound to mark the interrogation site, were used to definitively localize cavitation bubble activity to the renal parenchyma.[43] It has also been shown that renal injury in pigs is dramatically reduced when shock waves are administered using a pressure-release insert that suppresses cavitation.[10] Taken together, these data strongly support the idea that lithotripter shock waves produce cavitation *in vivo*, and that bubble activity plays a role in tissue damage.

Cavitation is also strongly implicated as a mechanism involved in stone fragmentation in SWL. *In vitro* studies have shown that damage to stones is dramatically reduced when the stones are treated while immersed in viscous media[5] or when shock waves are administered at overpressure sufficient to eliminate cavitation.[41]

If, as such studies suggest, cavitation contributes both to stone fragmentation and to tissue damage, strategies to control bubble activity could be very useful, especially if it were possible to find conditions that inhibit kidney trauma without interfering with stone comminution. Our observations help to explain how overpressure and PRF influence cavitation. We show that cavitation is dramatically affected by the presence of nuclei from previous shock waves, and that increased overpressure and reduced PRF allow those cavitation bubbles that are not stabilized by interactions with solid surfaces to dissolve between pulses.

Numerically, the time history of a bubble subjected to a lithotripter pulse was modeled from a synthesis of models by Church[24] and by Epstein and Plesset.[26] Rapid growth and collapse of the bubble was calculated with a numerical solution[24] of the Gilmore equation.[25] In this time of rapid motion of the air–water interface gas diffusion was approximated by Eller and Flynn's model[30] in which the thickness of the diffusion layer of the gas in the fluid is very small. At longer time, the thickness of the diffusion layer of gas could not be neglected, but the bubble radial velocity could. Then the equation by Epstein and Plesset[26] was used. The calculated lifetime t_L^* of a bubble was found to be fairly insensitive to initial bubble radius R_0 in the range 1–10 μm, because gas influx was much greater than initial gas constant of the bubble. Lifetime t_L^* was sensitive to static pressure p_0 and the peak acoustic driving pressure p_+, because in our wave form increased p_+ meant increased peak negative pressure p_-. Other factors are gas concentration in solution f and the diffusion coefficient D that depends on temperature and type of gas and liquid. These factors vary among *in vitro* and *in vivo* samples, and the effect of tissue constraint on our model has been described by Zhong *et al.*[9] Calculated bubble lifetime t_L^* and the duration of the growth and collapse cycle t_C^* are shortened by increasing static pressure p_0.

Lifetimes t_L for bubbles created by lithotripter pulses were measured by *B*-mode ultrasound and by high-speed camera. Lithotripter pulses created hyperechogenic regions in water within pipette bulbs. The disappearance of the hyperechogenic region was measured versus p_0 and compared very well to the calculated t_L^*. The lifetime of hyperechogenic regions at $p_0 = 1$ bar has previously been shown to be comparable *in vivo* and *in vitro*;[38,43] although in some *in vivo* locations, hyperecho is washed out of the region of interest by blood perfusion before bubbles dissolve.[33] High-speed camera images indicated that a dense cavitation cluster appeared when the time between shock waves (1/PRF) was less than the bubble lifetime (t_L). Measured t_L and calculated t_L^* were found to agree very well and both showed a sharp decay with increased static pressure p_0. However, measured lifetimes were reduced more strongly by overpressure than was predicted by calculated t_L^*. Our model assumed symmetric pulsation of a single bubble and did not account for bubble fragmentation. Thus the presence of a cluster of small bubbles was neglected. The equilibrium bubble radius may have been smaller because of asymmetry in collapse and splintering of one bubble into many daughter bubbles. Measurements with *B*-mode ultrasound showed that the hyperechoic region was brighter, larger, and denser with subsequent lithotripter pulses and with increasing PRF. Larger bubbles are more likely to collapse nonspherically

and break into smaller bubbles, which then grow. An increase in the number of bubbles after each shock wave would contribute to the brighter, larger, denser cluster. The very presence of several other bubbles may reduce both the gas diffusion into each bubble, as several bubbles compete for the gas dissolved in the fluid, and the pressure and inertia driving the growth and collapse of each bubble, as the cluster itself changes the compressibility of the fluid bubble mixture. Our measurements with the high-speed camera indicated that clusters were denser, bubbles were smaller, and collapse times longer at higher PRF. The measurements suggest that reduction of gas diffusion into each bubble, reduction of fluid outward motion, and reduction of pressure driving bubble collapse were the dominant effects of increased cluster density.

High-speed camera images showed that bubbles in the free field were considerably more sensitive to overpressure than those that formed along a crack in the glass slide used as a target. Thus, our observations support the concept[21,40,41] that bubbles appear to be stabilized by contact with cracks and crevices. Such stabilization of bubbles could explain why modest overpressure reduces damage to cells in suspension, but minimally suppresses stone fragmentation.[17]

Our observations imply that control of PRF and overpressure could be used to improve SWL in the clinical setting. In conventional lithotripsy treatment, low PRF may be used to allow bubble dissolution between pulses and thus to suppress cavitation *in vivo*. However, the duration of a lithotripsy procedure is limited by the rate of lithotripter pulse delivery. A treatment of 2000 pulses at 1 Hz requires over 30 min. Modest overpressure (1–3 bar) accelerates the dissolution of unstabilized bubbles such as those that can develop in the vasculature. Thus, it should be possible to use faster treatment rates without an increase in tissue damage. Since irregularities and cracks in the surface of kidney stones have the potential to stabilize bubbles against overpressure, it seems feasible that application of modest overpressure could reduce cavitation-mediated damage to tissue without interfering with the role that bubble activity plays in stone comminution.

ACKNOWLEDGMENTS

We thank Dr. James E. Lingeman (Methodist-Clarian Hospital) and Dr. Andrew P. Evan [Indiana University (IU) Medical School] for use of the Dornier HM-3 lithotripter at Methodist Hospital in Indianapolis. We thank Dr. Peter Kaczkowski [Applied Physics Lab (APL)] and Francis Olson (APL) for design and manufacture of the ''pressure-bottle'' pressure chamber, David Lounsbery (IU) for manufacture of the ''pressure cube,'' and Semih Sinik (Itronics Imaging Technologies, Westlake Village, CA) and Frank Kosel (DRS Hadland, Inc., Cupertino, CA) for technical advice with the high-speed camera. This work was supported by NIH Grant Nos. P01 DK43881, R01 DK55674, NIH Fogarty FIRCA, NATO, and CRDF.

[1] C. Renner and J. Rassweiler, ''Treatment of renal stones by extracorporeal shock wave lithotripsy,'' Nephron **81**, 71–81 (1999).
[2] A. P. Evan, L. R. Willis, J. E. Lingeman, and J. A. McAteer, ''Renal trauma and the risk of long-term complications in shock wave lithotripsy,'' Nephron **78**, 1–8 (1998).
[3] W. Sass, M. Braunlich, H. Dreyer, E. Matura, W. Folberth, H. Priesmeyer, and J. Seifert, ''The mechanisms of stone disintegration by shock waves,'' Ultrasound Med. Biol. **17**, 239–243 (1991).
[4] N. G. Holmer, L. O. Almquist, T. G. Hertz, A. Holm, E. Lindstedt, H. W. Persson, and C. H. Hertz, ''On the mechanism of kidney stone disintegration by acoustic shock waves,'' Ultrasound Med. Biol. **17**, 479–489 (1991).
[5] N. Vakil, S. M. Gracewski, and E. C. Everbach, ''Relationship of model stone properties to fragmentation mechanisms during lithotripsy,'' J. Litho. Stone Dis. **3**, 304–310 (1991).
[6] M. Kuwahara, N. Ioritani, K. Kamke, S. Shirai, K. Taguchi, T. Saitoh, S. Orikasa, K. Takayama, S. Aida, and N. Iwama, ''Hyperechoic region induced by focused shock waves *in vitro* and *in vivo*: Possibility of acoustic cavitation bubbles,'' J. Litho. Stone Dis. **1**, 218–228 (1989).
[7] A. J. Coleman, M. J. Choi, and J. E. Saunders, ''Detection of acoustic emission from cavitation in tissue during extracorporeal lithotripsy,'' Ultrasound Med. Biol. **22**, 1079–1087 (1996).
[8] D. Dalecki, C. H. Raeman, S. Z. Child, D. P. Penney, R. Mayer, and E. L. Carstensen, ''The influence of contrast agents on hemorrhage produced by lithotripter fields,'' Ultrasound Med. Biol. **23**, 1435–1439 (1997).
[9] P. Zhong, Y. Zhou, and S. Zhu, ''Dynamics of bubble oscillation in constrained media and mechanisms of vessel rupture in SWL,'' Ultrasound Med. Biol. **27**, 119–134 (2001).
[10] A. P. Evan, L. R. Willis, B. A. Connors, Y. Shao, J. E. Lingeman, J. C. J. Williams, J. A. McAteer, N. S. Fineberg, M. R. Bailey, and L. A. Crum, ''Kidney damage and renal functional changes are minimized by waveform control that suppresses cavitation in SWL,'' J. Urol. (in press).
[11] M. R. Bailey, D. T. Blackstock, R. O. Cleveland, and L. A. Crum, ''Comparison of electrohydraulic lithotripters with rigid and pressure-release ellipsoidal reflectors. II. Cavitation fields,'' J. Acoust. Soc. Am. **106**, 1149–1160 (1999).
[12] M. R. Bailey, ''Control of acoustic cavitation with application to lithotripsy,'' (Technical Report No. ARL-TR-97-1, Applied Research Laboratories, The University of Texas at Austin, Austin, TX, 1997, pp. 1–210.
[13] D. L. Sokolov, M. R. Bailey, and L. A. Crum, ''Use of a dual-pulse lithotripter to generate a localized and intensified cavitation field,'' J. Acoust. Soc. Am. **110**, 1685–1695 (2001).
[14] D. L. Sokolov, M. R. Bailey, F. Pulvermakher, and L. A. Crum, ''Increased damage to stones without increased damage to cells with a dual-reflector lithotripter,'' in Proceedings of the IEEE International Ultasonics Symposium, San Juan, Puerto Rico, 2000, Vol. 2, pp. 1437–1440.
[15] X. F. Xi and P. Zhong, ''Improvement of stone fragmentation during shock wave lithotripsy using a combined EH/PEAA shock wave generator—*in vitro* experiments,'' Ultrasound Med. Biol. **26**, 457–467 (2000).
[16] P. Zhong and Y. Zhou, ''Suppression of large intraluminal bubble expansion in shock wave lithotripsy without compromising stone comminution: Methodology and *in vitro* experiments,'' J. Acoust. Soc. Am. **110**, 3283–3291 (2001).
[17] M. Delius, ''Minimal static excess pressure minimises the effect of extracorporeal shock waves on cells and reduces it on gallstones,'' Ultrasound Med. Biol. **23**, 611–617 (1997).
[18] P. Huber, K. Jochle, and J. Debus, ''Influence of shock wave pressure amplitude and pulse repetition frequency on the lifespan, size and number of transient cavities in the field of an electromagnetic lithotripter,'' Phys. Med. Biol. **43**(10), 3113–3128 (1998).
[19] R. F. Paterson, D. A. Lifshitz, J. E. Lingeman, J. C. Williams, D. L. Rietjens, A. P. Evan, B. A. Connors, M. R. Bailey, L. A. Crum, R. O. Cleveland, Y. A. Pishchalnikova, I. V. Pishchalnikova, and J. A. McAteer, ''Slowing the pulse repetition frequency in shock wave lithotripsy (SWL) improves stone fragmentation *in vivo*,'' in Proceedings of the 17th International Congress on Acoustics, Rome, Italy, 2001, pp. 200–201.
[20] M. Delius, W. Mueller, A. Goetz, H.-G. Liebich, and W. Brendel, ''Biological effects of shock waves: Kidney hemorrhage in dogs at a fast shock wave administration rate of fifteen hertz,'' J. Litho. Stone Dis. **2**, 103–110 (1990).
[21] R. E. Apfel, ''The role of impurities in cavitation-threshold determination,'' J. Acoust. Soc. Am. **48**, 1179–1186 (1970).
[22] R. O. Cleveland, M. R. Bailey, L. A. Crum, M. A. Stonehill, J. C. Williams, Jr., and J. A. McAteer, ''Effect of overpressure on dissolution and cavitation of bubbles stabilized on a metal surface,'' in Proceedings of the 16th International Congress on Acoustics, Seattle, Washington, 1998, Vol. 3, pp. 2499–2500.

[23] M. R. Bailey, R. O. Cleveland, O. A. Sapozhnikov, J. A. McAteer, J. C. Williams, Jr., and L. A. Crum, ''Effect of increased ambient pressure on lithotripsy-induced cavitation in bulk fluid and at solid surfaces,'' in *Collected Papers from the Joint Meeting 'Berlin 99:' 137th Meeting of the Acoustical Society of America; 2nd convention of the European Acoustics Association; 25th German Acoustics DAGA conference*, edited by M. Moser and J. Tichy (Deutsche Gesellschaft fur Akustik (DEGA), Berlin, 1999), pp. 1–4 (CDROM only—no true page numbers).
[24] C. C. Church, ''A theoretical study of cavitation generated by an extracorporeal shock wave lithotripter,'' J. Acoust. Soc. Am. **86**, 215–227 (1989).
[25] F. R. Gilmore, ''The growth or collapse of a spherical bubble in a viscous compressible liquid,'' California Institute of Technology Report No. 26-4, 1952, pp. 1–40.
[26] P. S. Epstein and M. S. Plesset, ''On the stability of gas bubbles in liquid-gas solutions,'' J. Chem. Phys. **18**, 1505–1509 (1950).
[27] A. J. Coleman and J. E. Saunders, ''A review of the physical properties and biological effects of the high amplitude acoustic fields used in extracorporeal lithotripsy,'' Ultrasonics **31**, 75–89 (1993).
[28] S. Zhu and P. Zhong, ''Shock wave—inertial microbubble interaction: A theoretical study based on the Gilmore formulation for bubble dynamics,'' J. Acoust. Soc. Am. **106**, 3024–3032 (1999).
[29] F. Chavrier, J. Y. Chapelon, A. Gelet, and D. Cathignol, ''Modeling of high-intensity focused ultrasound-induced lesions in the presence of cavitation bubbles,'' J. Acoust. Soc. Am. **108**, 432–440 (2000).
[30] A. Eller and H. G. Flynn, ''Rectified diffusion during nonlinear pulsations of cavitation bubbles,'' J. Acoust. Soc. Am. **37**, 493–503 (1965).
[31] W. Press, S. A. Teukolsky, W. T. Vetterling, and B. R. Flannery, *Numerical Recipes in FORTRAN*, 2nd ed. (Cambridge University Press, Cambridge, 1992), pp. 704–716.
[32] R. O. Cleveland, M. R. Bailey, N. Fineberg, B. Hartenbaum, M. Lokhandwalla, J. A. McAteer, and B. Sturtevant, ''Design and characterization of a research electrohydraulic lithotripter patterned after the Dornier HM3,'' Rev. Sci. Instrum. **71**, 2514–2525 (2000).
[33] M. R. Bailey, L. N. Couret, O. A. Sapozhnikov, V. A. Khokhlova, G. ter Haar, S. Vaezy, X. Shi, R. Martin, and L. A. Crum, ''Use of overpressure to assess the role of bubbles in focused ultrasound lesion shape *in vitro*,'' Ultrasound Med. Biol. **27**, 696–708 (2000).
[34] M. A. Stonehill, J. C. Williams, Jr., M. R. Bailey, D. Lounsbery, R. O. Cleveland, L. A. Crum, A. P. Evan, and J. A. McAteer, ''An acoustically matched high pressure chamber for control of cavitation in shock wave lithotripsy: Mechanisms of shock wave damage *in vitro*,'' Methods Cell Sci. **19**, 303–310 (1998).
[35] R. O. Cleveland, O. A. Sapozhnikov, M. R. Bailey, and L. A. Crum, ''A dual passive cavitation detector for localized detection of lithotripsy-induced cavitation *in vitro*,'' J. Acoust. Soc. Am. **107**, 1745–1758 (2000).
[36] A. J. Coleman, M. J. Choi, J. E. Saunders, and T. G. Leighton, ''Acoustic emission and sonoluminescence due to cavitation at the beam focus of an electrohydraulic shock wave lithotripter,'' Ultrasound Med. Biol. **18**, 267–281 (1992).
[37] K. Jochle, J. Debus, W. J. Lorenz, and P. Huber, ''A new method of quantitative cavitation assessment in the field of a lithotripter,'' Ultrasound Med. Biol. **22**, 329–338 (1996).
[38] M. Delius, and S. Gambihler, ''Sonographic imaging of extracorporeal shock wave effects in the liver and gallbladder of dogs,'' Digestion **52**, 55–60 (1992).
[39] R. K. Zeman, W. J. Davros, B. S. Garra, J. A. Goldberg, S. C. Horii, P. M. Silverman, E. L. Cattau, W. S. Hayes, and C. J. Cooper, ''Cavitation effects during lithotripsy. II. Clinical observations,'' Radiology **177**, 163–166 (1990).
[40] A. A. Atchley and A. Prosperetti, ''The crevice model of bubble nucleation,'' J. Acoust. Soc. Am. **86**, 1065–1084 (1989).
[41] L. A. Crum, ''Nucleation and stabilization of microbubbles in liquids,'' Appl. Sci. Res. **38**, 101–115 (1982).
[42] J. A. McAteer, M. A. Stonehill, K. Colmenares, J. C. Williams, A. P. Evan, R. O. Cleveland, M. R. Bailey, and L. A. Crum, ''SWL cavitation damage *in vitro*: Pressurization unmasks a differential response of foil targets and isolated cells,'' Proceedings of the 16th International Congress on Acoustics and 135th Meeting of the Acoustical Society of America 1998, Vol. 3, pp. 2497–2498.
[43] M. R. Bailey, L. A. Crum, N. Miller, O. A. Sapozhnikov, Y. A. Pishchalnikov, R. O. Cleveland, J. A. McAteer, P. Blomgren, B. A. Connors, and A. P. Evan, ''Localized cavitation detection in lithotripsy *in vivo*,'' in Proceedings of the 17th International Congress on Acoustics, Rome, Italy, 2001, pp. 178–179.